Progress Towards a High-Resolution Retinal Prosthesis

Alex Butterwick*[a], Alex Vankov [a,b], Phil Huie [a,b], Karthik Vijayraghavan [a], Jim Loudin [a], Daniel Palanker [a,b]
[a]Hansen Experimental Physics Laboratory, Stanford University, Stanford, CA, USA 94305
[b]Department of Ophthalmology, Stanford University, Stanford, CA, USA 94305

ABSTRACT

Electronic retinal prostheses represent a potentially effective approach for restoring some degree of sight in blind patients with retinal degeneration. Functional restoration of sight would require hundreds to thousands of electrodes effectively stimulating remaining neurons in the retina. We present a design of an optoelectronic retinal prosthetic system having 3mm diameter retinal implant with pixel sizes down to 25 micrometers, which allows for natural eye scanning for observing a large field of view, as well as spatial and temporal processing of the visual scene to optimize the patient experience. Information from a head mounted video camera is processed in a portable computer and delivered to the implanted photodiode array by projection from the LCD goggles using pulsed IR (810 nm) light. Each photodiode converts pulsed light (0.5 ms in duration) into electric current with efficiency of 0.3 A/W using common bi-phasic power line. Power is provided by the inductively-coupled RF link from the coil on the goggles into a miniature power supply implanted between the sclera and the conjuctiva, and connected to subretinal implant with a thin 2-wire trans-scleral cable.

3-dimensional structures in the subretinal prosthesis induce retinal migration and thus ensure close proximity between stimulating electrodes and the target retinal neurons. Subretinal implantations of the 3-dimentional pillar and chamber arrays in RCS rats with 2 and 6 week follow-up demonstrate achievement of intimate proximity between the stimulation cites and the inner nuclear layer. In some instances formation of a fibrotic seal has been observed.

Keywords: Retinal Prosthesis, Neural Interface

1. INTRODUCTION

Many cases of intractable vision loss arise from selective photoreceptor degeneration. Retinitis pigmentosa (RP), for example, causes the loss of up to 95% of the photoreceptor layer, but spares up to 80% of the inner nuclear layer and ~ 30% of the ganglion cell layer[1, 2]. Similarly, patients with age-related macular degeneration (AMD) can lose up to 70% of photoreceptors with no loss of other retinal cell types. Approximately 1 in 4,000 newborns inherits the genotype for RP, while AMD, which arises from multiple causes including natural aging and environmental stresses, is diagnosed in 700,000 new Americans annually. While progression of AMD can be slowed (but not arrested), no treatment currently exists for RP. Electrical stimulation may be a potential treatment in cases of selective photoreceptor loss to artificially deliver visual information to the surviving retina, thereby bypassing the damaged neural tissue. Initial experiments have produced simple visual percepts such as spots and patterns by electrically stimulating the degenerated retina with just a few electrodes[3-5].

A large percentage of patients with age-related macular degeneration preserve visual acuity in the range of 20/400 and retain good peripheral vision. Implantation of an electronic prosthesis would be justified for such patients only if it provided substantial improvement in visual acuity. In contrast, patients with advanced retinitis pigmentosa would benefit little unless there was enough enlargement of the central visual field to allow reasonable ambulation. Normal visual acuity (20/20) corresponds to angular separation of lines by 1 minute of arc[6], or spatial separation on the retina of about 10 μm. To consistently resolve two lines separated by 10 μm requires 5 μm pixels (Nyquist sampling). Thus visual acuity at the level of 20/400 corresponds geometrically to a pixel size of about 100 μm, while acuity of 20/100 (sufficient for reading with some visual aids) requires pixels smaller than 25 μm. It has been previously estimated that

*butterwick@stanford.edu; phone +1 (650) 723-0789; 445 Via Palou, Stanford, CA 94305

about 600 pixels is a minimum for resolving images in the central field[7] and for useful reading performance[8]. For functional restoration of sight the array should ideally cover a field of view of at least 10^o (which corresponds to a 3 mm diameter spot on the retina), and support a visual acuity of 20/100 (which corresponds to 1600 pixels/mm^2) in the central 2-3^o of stimulating area.

2. SYSTEM DESIGN

As diagrammatically shown in Figure 1, a video camera transmits 640x480 pixel images at 25 – 50 Hz to a pocket PC. The computer processes the data and displays the resulting images on an LCD matrix mounted on goggles worn by the patient. The LCD screen is illuminated with pulsed near-infrared (NIR, 800-900 nm) light, projecting each image through the eye optics onto the retina. The NIR light is then received by a photodiode array on a ~3mm implanted chip. Each photodiode converts the NIR signal into an electric current, which is injected to the retina from an electrode placed in its center. Charge injection is maximized by biasing the photodiodes using a common pulsed biphasic power supply. Since the projected NIR image is superimposed onto a normal image of the scene observed through the transparent goggles, electrical stimulation introduces visual information into the retinal tissue above the implant, while any remaining peripheral vision responds normally to visible light. Such overlay is possible because NIR light does not activate normal photoreceptors and the implant's response to natural visible light in the eye is negligible compared to the bright and pulsed infrared image.

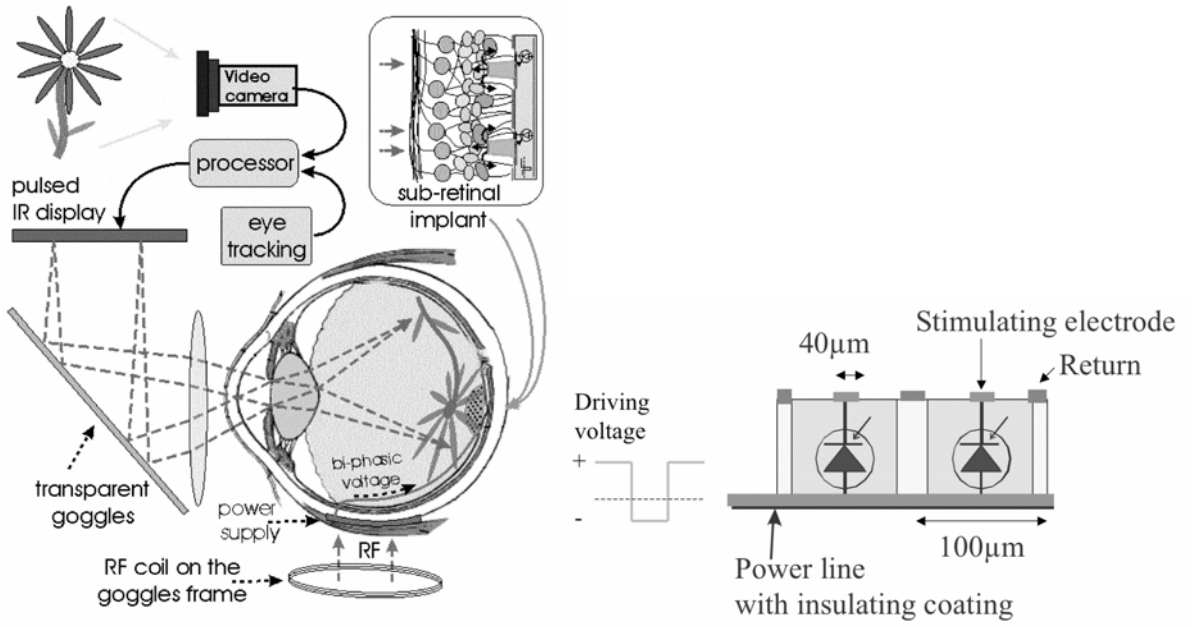

Fig. 1. Schematic of retinal prosthesis system. The visual scene, shown in the top left corner, is recorded with a video camera. A pocket PC, which tracks the gaze of the patient, determines the region of the scene that falls on the photodiode-based implant and is able to do image processing that improves the patients perception. The transformed video frame is projected, in infrared light, to the implant, while the use of transparent goggles allows the normal function of the remaining photoreceptors. The image that is projected onto the implant is transduced by local photodiodes to an electrical stimulating current these photodiodes are powered by an implanted RF coil. On the right is a schematic of the photodiode and electrode.

Advantages of this system over other current approaches to visual prosthesis include:

- Optical projection of the images into the eye preserves the natural link between eye movements and visual information. Since the video goggles can project images onto a retinal area much larger than the chip itself, the

patient can observe a larger field of view with natural eye movements rather than by scanning it with his head-mounted camera.

- Each photodiode acts as a separate data channel, allowing parallel optical transmission of information during stimulation. In contrast, single channel systems must transmit data serially, necessitating complex data decoding and memory circuitry in the implant, as well as a multiplicity of wires connecting this circuitry to the electrode array[4, 9-11].
- Adjustment of the stimulation parameters (intensity, duration, and repetition rate) and the image processing algorithm can be performed for each patient without any changes in the retinal chip itself, as opposed to systems where signal processing is built into the implant itself [12].
- The system can be used for both epiretinal and subretinal stimulation.

A possible disadvantage of this system is that presence of photodiodes in series with the electrodes prevents application of some types of stimulation waveforms, such as symmetric biphasic current pulses (equal current pulses of opposite polarity).

The threshold charge required to electrically elicit an action potential in retinal ganglion cells depends on electrode size and distance from the target cells[13, 14]. Thresholds for human perception of retinal stimulation with large epiretinal electrodes - disks of 520 μm in diameter - have been determined to be in the range 50 to 500 nC for biphasic current pulses with 1 ms per phase[5]. With electrodes of 6-25 μm in size placed on the epiretinal surface of the rabbit retina the threshold for eliciting an action potential in the ganglion cells was found to be in the range of 0.05-0.3 nC [13, 15]. With 125 μm diameter electrodes it varied from 0.3 to 3 nC for different types of cellular responses[14]. With 0.5 ms pulses the threshold current varied from 0.4 to 4 μA [14]. In subretinal stimulation using 10 μm electrodes and 0.5 ms pulses the stimulation threshold was in the range of 0.4-0.7nC, which corresponds to a threshold current of 0.8 – 1.4 μA[16].

Our first generation implant has 100 μm square photodiode pixels, each with a 40 μm diameter circular electrode in its center. Based on the stimulation thresholds cited above we plan to provide 0.5 ms stimulation pulses with currents up to 20 μA per pixel, which is 5 times lower than the retinal damage threshold for electrodes smaller than 100 μm in diameter[17]. This stimulation current corresponds to 10 nC injected per pulse and a maximum electrode charge density of 0.8 mC/cm^2. Since this charge density exceeds the safe limit for platinum electrodes (0.4 mC/cm^2 [18, 19]) we use activated iridium oxide film (AIROF) electrodes, which have a safe charge-injection limit of 1-9 mC/cm^2[20].

The electric field produced by a disk electrode with constant current density at its surface is nearly flat and distance-independent in the near-field, and spherical in the far field. The transition between the two regimes occurs at distances comparable to electrode size. In the far-field range the electric field decreases quadratically with distance from the plane of electrode. Given that electrode-cell separation is typically 20-40 μm for flat epiretinal and subretinal implants, our 40 μm electrodes could effectively stimulate ganglion cells with a flat epiretinal array, or inner nuclear layer cells with a flat subretinal array. The use of smaller electrodes at the same distance from the target cells would necessitate higher electrode current density to provide a similar current in the far-field. Since electrochemically-safe current density is limited, better proximity to target cells is essential for high resolution stimulation. New techniques we have developed to achieve cellular-scale proximity are discussed below.

2.1 Photovoltaic and photoconductive modes of operation

Each pixel consists of a photodiode in series with the stimulating electrodes, because the photodiode conducts in one polarization but is a variable, light intensity-controlled current limiters in the other, it isn't possible to deliver symmetric biphasic pulses with two sequentially-activated constant-current pulses of opposite polarities. However, biphasic stimulation is necessary for safe chronic operation of the electrodes. To get a charge-balanced biphasic pulse with this setup there are two practical solutions: use voltage-controlled stimulation with current-controlled biasing, or current controlled stimulation with voltage-controlled biasing. The former can be though of as a "continuous illumination" mode, since the light is the biasing current source, and the latter as a "pulsed illumination" mode, in which current is controlled by light applied in brief pulses. Though, photodiode polarity is hardwired into the implant, both anodic-first and cathodic-first stimulation pulses are possible. In the pulsed illumination mode, the photoconducting (reverse) polarity for is used for stimulation, while continuous illumination mode uses the conducting (forward) polarity for

stimulation. The ability to switch between stimulus polarities is controlled by the NIR projection system and its synchronization with the RF biasing system, and can be changed at any time after implantation.

In the pulsed illumination mode biasing phase, the active bias circuitry uses the conducting polarization of the diode to charge the electrochemical capacitance of the electrode-electrolyte interface. Next, during the "stimulation" phase, this capacitor is discharged via the light-controlled conduction of the photodiode. During this phase, the photodiode is fully reverse biased, to the voltage water window, and the resulting current comes from the photogenerated electron-hole pairs in the photodiode.

Conversely, the continuous illumination mode charges the electrochemical capacitor with the current limited polarization of the diode. During the stimulus phase, the capacitor is rapidly discharged with the conducting polarization of the diode. Because the current generation phase of the photodiode extends over the interpulse period, 20–40 ms, in the continuous illumination mode, much less peak light power is needed to operate, though the average energy per stimulus cycle is the same in both modes.

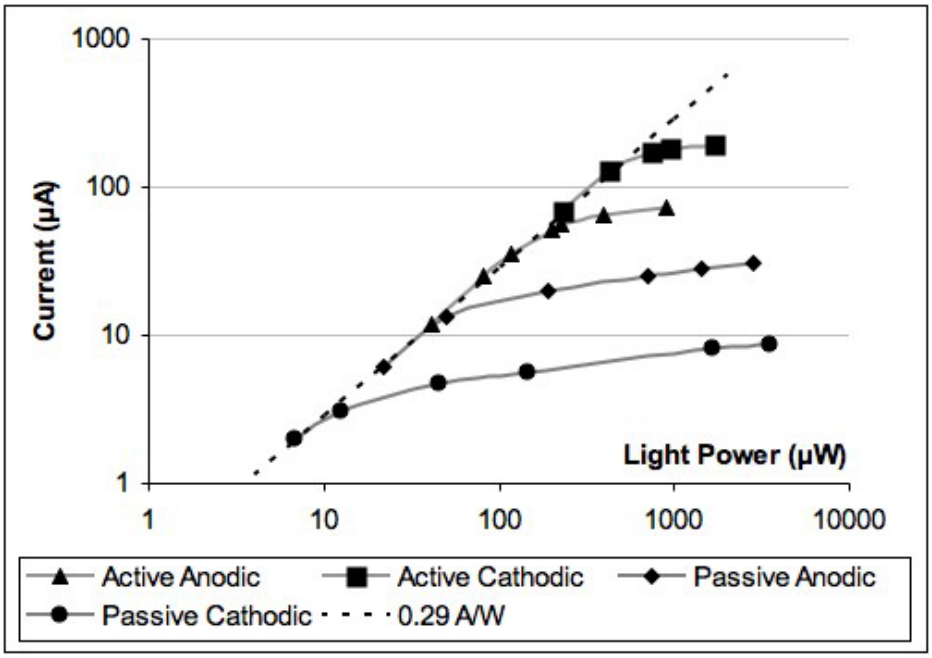

Fig. 2. Optoelectronic performance of photodiodes in both active and passive operation. Active operation of the photodiode gives the prosthesis greater dynamic range.

If stimulation thresholds are sufficiently low, passive operation of the implant is sufficient, however, for a wider dynamic range, or to stimulate neurons with a higher stimulation threshold, an active system will be used. A comparison of the performance of the photodiodes in both modes is presented in figure 2. In the initial current-limited phase of operation the curves are all linear, as expected. The slope of the curves in this regime, 0.29 A/W, is the photodiode conversion efficiency. The saturation behavior is explained by the logarithmic dependence of the photovoltage on light intensity.

2.2 Optical Design

To deliver the high peak powers necessary for each pixel to deliver 0.2 to 20 µA of stimulus current in 0.5 ms pulses, careful attention needs to be paid to the collimating optics and light sources used in the projection system. As mentioned earlier, the irradiance required for the 3 mm diameter implant to stimulate the retina is 2.5 mW/mm^2 peak and 62µW/mm^2. For comparison of scale, the eye typically receives 1µW/mm^2 when looking at a bright object on a sunny day. IR light is a good choice for projecting this level of power onto the retina considering it is safe to the exposed

tissues, photodiodes can be fabricated with good IR sensitivity, there are a number of solid-state IR light sources available, and visible wavelengths would quickly saturate remaining photoreceptors.

Receiving 3.5 mW/mm^2 with the focal lengths of the eye, f, and the ocular, F, defines the LCD irradiance as $I = I_0 \cdot \left[\frac{f}{F}\right]^2$. The corresponding LCD display brightness is $B = \frac{I}{\Omega}$ where $\Omega = \frac{\pi}{4} \cdot \left[\frac{d}{F}\right]^2$ is the acceptance angle determined by the ocular focal length F and pupil diameter d. Due to inevitable optical losses the actual surface brightness must be significantly larger than the minimum: $B > \frac{4I_0}{\pi}\left[\frac{f}{d}\right]^2$. Since typically d~3mm and f~17mm, the minimal brightness is 0.2 W/mm^2/sr.

Laser diodes (LD) are able to supply enough light, but the high spatial coherence of the output light causes constructive and destructive interference, and hence a highly uneven beam profile. For the retinal prosthesis system, the beam profile must be very close to constant across the implant. This assures that the amount of light falling on the implant, and the corresponding electrical stimulus, is independent of the orientation of the implant in the projected image. Speckling in the profile beam would cause unpredictable amounts of current in the stimulus over the area of the implant.

Suppressing the amount of interference my decreasing the spatial coherence of the output from the light source is necessary to maintain an even intensity profile across the beam. Our design includes using multiple LDs coupled into a long stretch of a multimode decreases pixel-to-pixel variations in light intensity on the retinal array to less than 1%, allowing full utilization of the dynamic range provided by the light modulator. A light homogenizer and a field lens, depicted in figure 3, help create a "flat top" beam profile on the LCD screen.

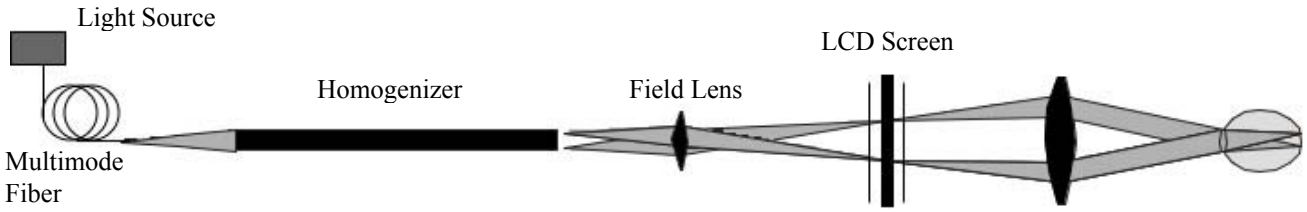

Fig. 3. Layout of optical components used in the system to provide sufficient peak power while suppressing speckling from the laser diodes on the implant.

2.3 Layout of the electrode array.

Specific pixels are activated by the NIR projection; however, cellular stimulation depends on the electric field created by the electrode array. Since the electrodes are activated simultaneously, the electric field of all active electrodes will be superimposed upon all other electrodes. Consequently, if the electrode array isn't designed correctly, the electric field near any electrode becomes strongly dependent on the activation of neighboring electrodes. A high-resolution implant requires that the electric field can be highly localized minimizing collateral stimulation of neurons from distant electrodes.

A simplified, analytically solvable model is useful to derive basic scaling laws of the effects on stimulation thresholds of cells when activating a large number of electrodes simultaneously. We start by considering a sphere (rather than a disk) emitting current from its whole surface at the same current density as the real implant (20 μA per 100μm pixel). In this case the total current injected from the sphere increases quadratically with its radius $I \sim r^2$, while the resistance between the spherical electrode and infinity decreases reciprocal to its radius $R \sim 1/r$. Thus the resistive potential drop between the sphere and the return at infinity, $U=I \cdot R$, will increase linearly with its radius, $U \sim r$. Since the total number of pixels $N \sim r^2$, we have the scaling law $U \sim N^{1/2}$. Consequently, an increase in size of the electrode array or the number of simultaneously activated pixels (assuming constant current per pixel) is accompanied by an increase in resistive voltage drop in the electrolyte. Given that our driving voltage is limited (-0.8 to 0.6V with respect to Ag/AgCl), these larger

resistive losses decrease the potential available at the electrode/electrolyte junction and thus the attainable charge injection.

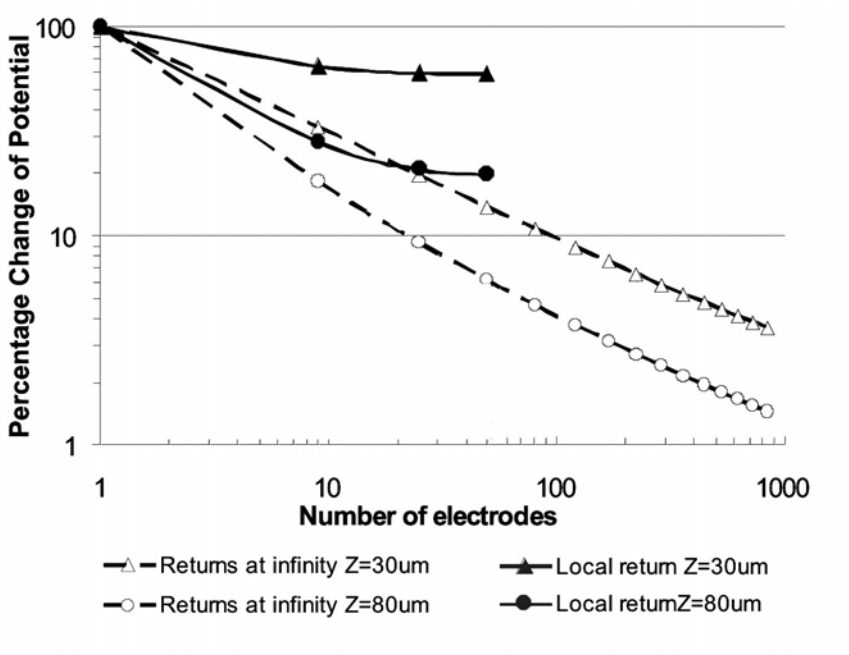

Fig. 4. Comparison of the relative change in electric potential, at two distances from the array, when one electrode is turned off. Computer simulations were done on square electrode arrays of various dimensions—with only one electrode the change in potential above it is 100%, however, when more electrodes are added to the array the accumulation of potential from other electrodes diminishes the change in potential when one electrode is turned off. When a local return is used, solid lines, the modulation is considerably better for a high resolution implant—requiring 1000's of electrodes, than having the return at infinity, dashed lines.

Now we look at the *relative change in electric potential* at 30 and 80 μm above a central electrode when many surrounding electrodes are activated. Simulations were run with constant total injected current from the electrodes and the return electrode placed at infinity; arrays size varied from 1 electrode to 841 (29^2). Figure 4 is the results of the simulations; the *relative change in electric potential* when one electrode is turned off is plotted. For example, with an array of only 1 electrode, the change in electric field when it is turned on and off is 100%. However, with 841 pixels the relative change in potential is only 3% 30μm above the center electrode and less than 2% when the separation is 80μm. When the return electrode is moved from infinity to the perimeter of each 100 μm photodiode, the change in potential for large arrays stays at 60%. Unfortunately, close proximity of the return electrode, used to reduce interference between electrodes, reduces the field's penetration depth into the tissue—i.e., by limiting the lateral spread we reduce the axial spread. A proposed method to keep the electrodes in close proximity to retinal neurons is described below. For comparison, figure 5 shows the electric potential in a cross-section in the center of a 3x3 array of electrodes. It compares the state with 9 electrodes on, left column, and with 8 perimeter electrodes on and the center electrode off, for arrays without a local return, top row, and with local returns, bottom row. Without the local return there is little change in the electric field when the center electrode is turned off. However, the field is well confined with local returns, and the electric field changes considerable between the two states.

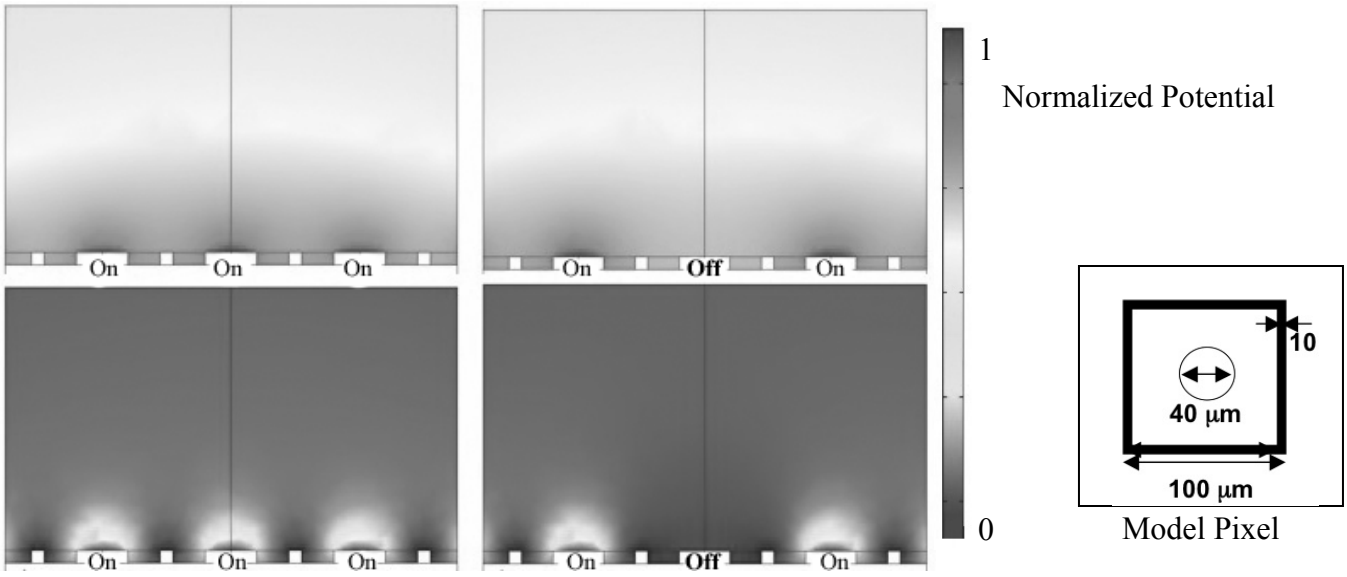

Fig. 5. Results of electric field simulations from a 3x3 array of electrodes. The top figures have an electrical return at infinity while the local return is used on the bottom figures. Figures in the left column have all nine electrodes on, while the simulations in the right column are done with the center electrode turned off.

2.4 Pillar electrodes

The electric field roughly penetrates a depth comparable to the size of the electrodes, demonstrated above in figure 5. However, planar implants placed at the epi-retinal surface will not be able to penetrate to the ganglion cell layer as electrode sizes shrink. For sub-retinal implants, cellular debris associated with the progression of retinal dystrophies keep the implant at least 20— 50μm from the inner nuclear layer. For a high resolution implant 3-dimensional implants can be used to keep even small electrodes sufficiently close to targeted neurons. For example, an array of pillars of about 10 μm in diameter and 40 – 70 μm in height, with active electrodes on the top of the pillars and return electrodes at the base, would allow targeted stimulation of cells at the desired retinal depth. Pillar arrays were tested using SU-8 polymer implants in RCS rats, a genetic animal model of retinal dystrophy. An example of the devices used for implantation and tissue reaction studies are shown in Figure 6.

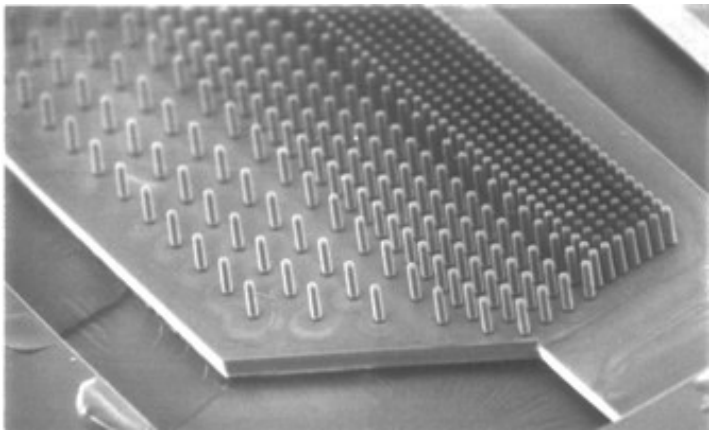

Fig. 6. SEM of SU-8 polymer implants that are designed to target the inner nuclear layer. Pillars are 10 μm in diameter and 50 μm tall.

Figure 7a shows histological micrographs of the results from implantation into the rat retina with both a flat, 45 μm thick implant 6 weeks post implantation. The devices were implanted in rats where the photoreceptors and most of the nuclei of the outer nuclear layer have degenerated, while the ganglion cell layer (GCL), the inner plexiform layer (IPL), the inner nuclear layer (IN) with some remnant nuclei of degenerated photoreceptors still remain. The upper surface of the subretinal implant is covered with a preretinal fibrotic membrane about 10 μm thick and a layer of hypotrophied Mueller cell processes. The inner nuclear layer is separated from the implant by approximately 40 μm.

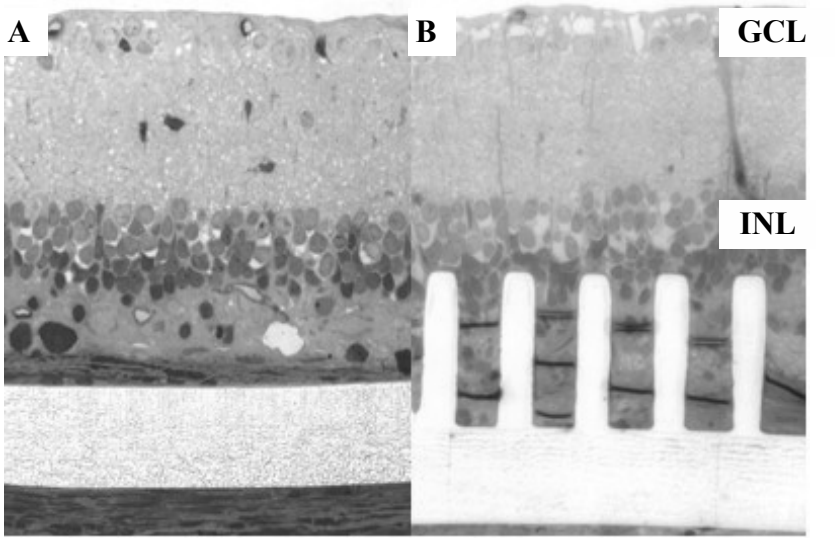

Fig. 7. SU-8 structures 6 weeks after implantation in RCS rats. The electrode surface is approximately 40 μm from the inner nuclear layer (INL) with the planar electrode geometry, figure 7A. Using 3-dimensional implants allows the pillar electrodes, figure 7b, to penetrate to within a couple microns of the INL. Additionally, pillar implants appear to suppress the development of cellular fibrosis around the implant.

Figure 7B shows a histological section of an RCS rat retina with a pillar implant 6 weeks post implantation. The 65 μm pillars penetrate into the middle of the INL, while all the inner retinal layers still appear well-defined. It is apparent that tissue migration around and towards the pillars during the first few days after the implantation provides relatively atraumatic penetration of the pillars into the INL, without significantly altering retinal architecture. In addition to providing closer proximity to the target cells, pillar structures seem to decrease the likelihood of fibrotic seal encapsulation of the electrodes. These findings should be further confirmed in the longer follow-ups, and in experiments involving chronic stimulation.

3. CONCLUSION

We have presented the design and specifications of an optoelectronic retinal prosthesis in which visual information is simultaneously delivered to hundreds of stimulating pixels by sequentially projecting individual video frames onto the implant using pulsed near-infrared light. Actively biasing the photodiodes in the retinal implant increases the AIROF electrode charge injection (compared to a passive system) by a factor of 4 for anodic-first pulses and by a factor of 40 for cathodic-first pulses. The bi-phasic biasing waveform is provided by an inductively powered pulse generator placed in the subconjuctival space. Anodic-first and cathodic-first stimulation pulses are both available: one is provided by the continuous illumination mode and the other by the pulsed illumination mode. Work is currently underway to construct a "first generation" implant with 100 μm pixels, although the same system design can be used with pixel sizes as small as 25 μm. Local return electrodes surrounding each pixel decouple electric fields of neighboring electrodes thereby decreasing cross-talk and interference, but place more stringent requirements on electrode-cell proximity. Intimate proximity can be achieved using 3-dimensional subretinal implants with pillar electrodes.

REFERENCES

1. Flannery, J.G., et al., *Degenerative changes in a retina affected with autosomal dominant retinitis pigmentosa.* Invest Ophthalmol Vis Sci, 1989. **30**(2): p. 191-211.

2. Stone, J.L., et al., *Morphometric analysis of macular photoreceptors and ganglion cells in retinas with retinitis pigmentosa.* Arch Ophthalmol, 1992. **110**(11): p. 1634-9.

3. Weiland, J.D. and M.S. Humayun, *Intraocular retinal prosthesis. Big steps to sight restoration.* IEEE Eng Med Biol Mag, 2006. **25**(5): p. 60-6.

4. Rizzo, J.F., 3rd, et al., *Perceptual efficacy of electrical stimulation of human retina with a microelectrode array during short-term surgical trials.* Invest Ophthalmol Vis Sci, 2003. **44**(12): p. 5362-9.

5. Humayun, M.S., et al., *Visual perception in a blind subject with a chronic microelectronic retinal prosthesis.* Vision Research, 2003. **43**(24): p. 2573-81.

6. Smith, G. and D.A. Atchison, *The Eye*, in *The Eye and Visual Optical Instruments*. 1997, Cambridge University Press: Cambridge. p. 291-316.

7. Margalit, E., et al., *Retinal prosthesis for the blind.* Survey of Ophthalmology, 2002. **47**(4): p. 335-356.

8. Sommerhalder, J., et al., *Simulation of artificial vision: II. Eccentric reading of full-page text and the learning of this task.* Vision Res, 2004. **44**(14): p. 1693-706.

9. Eckmiller, R., R. Hünermann, and M. Becker, *Exploration of a dialog-based tunable retina encoder for retina implants.* Neurocomputing, 1999. **26-27**: p. 1005-1011.

10. Mahadevappa, M., et al., *Perceptual thresholds and electrode impedance in three retinal prosthesis subjects.* IEEE Trans Neural Syst Rehabil Eng, 2005. **13**(2): p. 201-6.

11. Hornig, R., et al., *A method and technical equipment for an acute human trial to evaluate retinal implant technology.* J Neural Eng, 2005. **2**(1): p. S129-34.

12. Gekeler, F. and E. Zrenner, *[Status of the subretinal implant project. An overview]*. Ophthalmologe, 2005. **102**(10): p. 941-9.

13. Jensen, R.J., et al., *Thresholds for activation of rabbit retinal ganglion cells with an ultrafine, extracellular microelectrode.* Investigative Ophthalmology & Visual Science, 2003. **44**(8): p. 3533-43.

14. Jensen, R.J., O.R. Ziv, and J.F. Rizzo, 3rd, *Thresholds for activation of rabbit retinal ganglion cells with relatively large, extracellular microelectrodes.* Invest Ophthalmol Vis Sci, 2005. **46**(4): p. 1486-96.

15. Sekirnjak, C., et al., *Electrical stimulation of mammalian retinal ganglion cells with multielectrode arrays.* Journal of Neurophysiology, 2006. **95**(6): p. 3311-3327.

16. Stett, A., et al., *Electrical multisite stimulation of the isolated chicken retina.* Vision Research, 2000. **40**(13): p. 1785-1795.

17. Butterwick, A.F., et al. *Dynamic range of safe electrical stimulation of the retina*. in *Ophthalmic Technologies XVI*. 2006. San Jose, California.

18. Hesse, L., et al., *Implantation of retina stimulation electrodes and recording of electrical stimulation responses in the visual cortex of the cat.* Graefes Archive for Clinical and Experimental Ophthalmology, 2000. **238**(10): p. 840-845.

19. Robblee, L.S., et al., *Electrical-Stimulation with Pt Electrodes .5. The Effect of Protein on Pt Dissolution.* Biomaterials, 1980. **1**(3): p. 135-139.

20. Cogan, S.F., et al., *Potential-biased, asymmetric waveforms for charge-injection with activated iridium oxide (AIROF) neural stimulation electrodes.* Ieee Transactions on Biomedical Engineering, 2006. **53**(2): p. 327-332.